

# International Conference on Space Optics—ICSO 2012

Ajaccio, Corse

9–12 October 2012

*Edited by Bruno Cugny, Errico Armandillo, and Nikos Karafolas*



## *Extremely stable piezo mechanisms for the new gravitational wave observatory*

*Joep Pijnenburg*

*Niek Rijnveld*

*Harm Hogenhuis*



# Extremely stable piezo mechanisms for the New Gravitational wave Observatory

Joep Pijenburg<sup>a</sup>, Niek Rijnveld<sup>a</sup>, Harm Hogenhuis<sup>a</sup>  
<sup>a</sup>TNO Opto Mechatronics, Stieltjesweg 1, 2600 AD, Delft, The Netherlands  
Joep.Pijenburg@TNO.nl

**Abstract**— Detection and observation of gravitational waves requires extreme stability in the frequency range 3e-5 Hz to 1 Hz. NGO/LISA will attain this by creating a giant interferometer in space, based on free floating proof masses in three spacecrafts.

To operate NGO/LISA, the following piezo mechanisms are developed:

## 1. A piezo stack mechanism (Point Angle Ahead Mechanism)

Due to time delay in the interferometer arms, the beam angle needs to be corrected. A mechanism rotating a mirror with a piezo stack performs this task. The critical requirements are the contribution to the optical path difference (less than 1.4 pm/√Hz) and the angular jitter (less than 8 nrad/√Hz).

## 2. A piezo sliding mechanism (Fiber Switching Unit Actuator)

To switch from primary to the redundant laser source, a Fiber Switching Unit Actuator (FSUA) is developed. The critical requirements are the coalignment of outgoing beams of <+/-1 micro radian and <+/-1 micro meter. A redundant piezo sliding mechanism rotates a wave plate over 45 degrees.

## 3. A piezo stepping mechanism (In Field Pointing Mechanism)

Due to seasonal orbit evolution effects, beams have to be corrected over a stroke of +/-2.5 degrees. The critical requirements are the contribution to the optical path difference (less than 3.0 pm/√Hz) and the angular jitter (less than 1 nrad/√Hz). Due to the large stroke, a piezo stepping concept was selected. Dedicated control algorithms have been implemented to achieve these challenging requirements.

This paper gives description of the designs and the ongoing process of qualifying the mechanisms for space applications.

**Keywords:** piezo, sliding, stepping, picometer stability, control, elastic precision mechanism

## I. INTRODUCTION

The objective of the NGO/LISA mission is to observe and measure gravitational waves. Because of the extreme stability and low disturbance requirements, the detector will be created in space. The detector will consist of a giant interferometer with three measurement arms, travelling between three spacecraft each at a distance of 5 million kilometers from each other. Each spacecraft holds two free-floating proof masses, which provide the absolute reference for the interferometer arms. Because the disturbances acting on the proof masses are absolutely minimized, any path length changes measured by the interferometer arms can be attributed to gravitational waves. [1,2,8]

## II. POINT ANGLE AHEAD MECHANISM

### A. INTRODUCTION

Due to time delay in the interferometer arms, the direction of transmitted light changes. To solve this problem, a picometer stable Point-Ahead Angle Mechanism (PAAM) was designed, realized and successfully tested. The PAAM concept is based on a rotatable mirror. The critical requirements are the contribution to the optical path length (less than 1.4 pm / rt Hz) and the angular jitter (less than 8 nrad / rt Hz). Extreme dimensional stability is achieved by manufacturing a monolithical Haberland hinge mechanism out of Ti<sub>6</sub>Al<sub>4</sub>V, through high precision wire erosion. Extreme thermal stability is realized by placing the thermal center on the surface of the mirror. Because of piezo actuator noise and leakage, the PAAM has to be controlled in closed-loop. To meet the requirements in the low frequencies, an active target capacitance-to-digital converter is used. Interferometric measurements with a triangular resonant cavity in vacuum proved that the PAAM meets the requirements.

Due to the evolution of the orbit during its trip around the sun, the laser beam angles have to be corrected for constantly. Not only the in-plane angles are affected, but also the so-called point-ahead angles, which correct for the offset caused by the time delay of the travelling light. The Point-Ahead Angle Mechanism (PAAM) is designed to perform the task of correcting the point-ahead angle.

The PAAM is developed and tested by TNO Science & Industry, with the help of the Albert-Einstein-Institute in

Hannover. As an Elegant Bread-Board (EBB), it has successfully gone through all performance and environmental testing and is ready to be integrated in a functional breadboard of the Optical Bench for a LISA spacecraft.

**B. Driving requirements for the PAAM**

The PAAM is required to steer the incoming laser beam through a range of  $\pm 824 \mu\text{rad}$ , while contributing minimally to the optical path delay (OPD) and contributing minimally to the angular jitter of the laser beam angle. During operation, the mechanism will follow an annual trajectory that runs through the entire range twice.

**1) Performance requirements**

Both the specification for the optical path delay (OPD) and the angular jitter are described using a noise shape function, as shown Equation 1.

$$n(f) = \sqrt{\left(1 + \frac{2.8\text{mHz}}{f}\right)^4} \quad (1)$$

The requirements for OPD and angular jitter, defined in terms of amplitude spectral density (ASD), are multiplied with this noise shape function. It is designed such that the requirements are relieved below 2.8 mHz, and constant above this frequency. The requirements only apply within the LISA measurement band width, which is defined to be between 0.03 mHz and 1 Hz. Table 1 shows the requirements for OPD and angular jitter.

Performance requirements		
Description	Requirement	Unit
Optical Path Delay	$1.4 \cdot n(f)$	$\frac{\text{pm}}{\sqrt{\text{Hz}}}$
Angular jitter	$16 \cdot n(f)$	$\frac{\text{nrad}}{\sqrt{\text{Hz}}}$

Table 1: Performance requirements for the PAAM.

**2) Environmental requirements**

Several additional requirements make the design of the PAAM quite challenging. First of all, due to the sensitivity of the measurement set-up on the Optical Bench, no magnetic materials are allowed. This rules out the use of any electromagnetic actuators or bearings. Second, due to the strict requirements on stray light, the contamination requirements on the Optical Bench are extremely strict. Any outgassing materials, as well as mechanisms containing moveable parts with frictional contacts are to be avoided. Third, the mechanism will have to survive launch loads of 25 g RMS, without the use of a launch locking mechanism.

**C. Point-Ahead Angle Mechanism design description**

The PAAM consists of a mirror on a flexible rotational hinge, which can be actuated individually by either one of two piezo stacks. The angle is measured by a capacitive sensor. The system operates in closed loop. The overall design is shown in Top, and its realization is shown in Bottom. In the paragraphs below, the optical, mechanical and electrical design is described in detail.

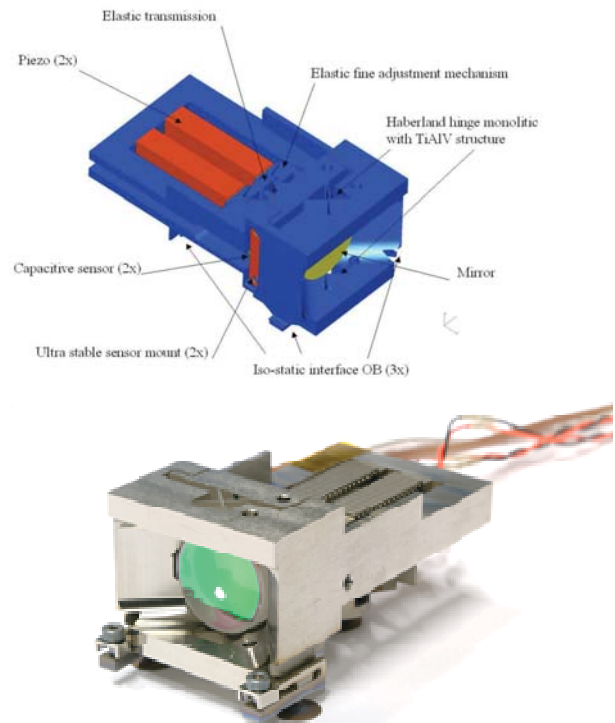


Figure 1. Top: CAD design of the Point-Ahead Angle Mechanism as designed by TNO Optomechatronics, including all its components. Bottom: Realization of the Point-Ahead Angle Mechanism. The mirrors can be actuated by one of two piezo-stacks. The mirror is mounted with a bonded iso static mount design for details see [6].

**D. Optical design**

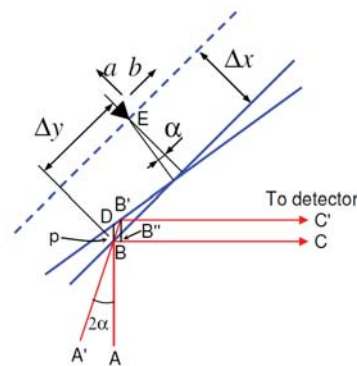


Figure 2: Schematic representation of the influence of alignment and jitter parameters of the mirror on the optical path delay of the incoming laser beam.

The optical concept for the PAAM is a mirror rotating around an axis in the mirror plane. This concept is chosen over alternatives due to its low transmission losses and low complexity. The mirror is coated for the wavelength of 1064 nm and for the incoming angle of 45°. The reflectivity is specified as more than 99.9%, and its flatness is better than 12 nm RMS over its entire diameter of 19.05 mm.

The Optical Path Delay (OPD) has been identified as the most critical requirement. If the laser beam and the reflecting surface are perfectly aligned with the rotation, the OPD due to rotation is theoretically zero. Figure 2 schematically shows the optical path delay due to a rotation of the mirror, when the beam and surface are not perfectly aligned.

From Figure 2 it can be seen that the OPD equals the distance BB'-BB". For small angles, this can be approximated by BD. The sensitivity of the distance BD, and hence the OPD, to the most relevant parameters is listed in **Error! Reference source not found.** These parameters are the angular jitter, caused by rotation of the mirror around the optical axis in combination with an alignment offset, the longitudinal jitter, caused by piston sensitivity and angular jitter, and the rotation axis longitudinal jitter, caused by parasitical actuation forces through the Haberland hinge. Other misalignments of the optical axis and cross-couplings were shown to have negligible contribution to the Optical Path Delay.

Sensitivity of the OPD to relevant parameters				
Param.	Description	Budget	Relation	Effect on OPD $pm/\sqrt{Hz}$
$\Delta x$	Static longitudinal misalignment	$\pm 1000 \mu m$	-	0
$\Delta y$	Static lateral misalignment	$\pm 50 \mu m$	-	0
$\Delta \alpha$	Angular jitter	$\frac{8 \cdot n(s)}{nrad/\sqrt{Hz}}$	$\delta BD = \sqrt{2}(\Delta x \alpha + \Delta y) \delta \alpha$	$0.57 \cdot n(s)$
$\delta \Delta x$	Longitudinal jitter	$\frac{0.28 \cdot n(s)}{pm/\sqrt{Hz}}$	$\delta BD = \sqrt{2}(1 + 0.5 \alpha^2) \delta \Delta x$	$0.40 \cdot n(s)$
$\delta \alpha$	Rotation axis longitudinal jitter	$\frac{0.30 \cdot n(s)}{pm/\sqrt{Hz}}$	$\delta BD = \sqrt{2} \delta \alpha$	$0.43 \cdot n(s)$
<b>Total</b>				<b>1.40 · n(s)</b>

Table 2: Sensitivity of the OPD to relevant parameters

E. Mechanical design

The rotation of the mirror is guided by a so-called Haberland hinge, a monolithic elastic cross hinge. Due to the limitations on magnetic materials and contamination, magnetic, hydrostatic or contact bearings are not favored. The axis of rotation of the Haberland hinge is aligned with the mirror surface.

The material of choice is Ti<sub>6</sub>Al<sub>4</sub>V, due to its high allowable stress and high dimensional stability. The mechanical design is

shown in Figure 1. The entire mechanism, excluding the functional components, is wire-eroded in a single fixture configuration; such that optimal production tolerances are achieved.

A compact elastic transmission between the actuator and mirror allows actuation of the mirror angle without introducing parasitic forces. The elastic transmission also enables the inclusion of a second, independent actuator, such that the mechanism is redundant. The required mechanical stroke of  $\pm 412 \mu rad$  can be actuated with an actuator stroke of 20  $\mu m$ , with minimal hysteresis effects.

To minimize OPD due to temperature variations, the thermal center of the Ti<sub>6</sub>Al<sub>4</sub>V structure is placed in line with the axis of mirror rotation. This is achieved by strategic placement of isostatic interfaces to the optical bench.

A finite-element model analysis (FEM) of the Haberland hinge was used to predict the longitudinal jitter, caused by the coupling between angular jitter and piston sensitivity. Production tolerances of  $\pm 10 \mu m$  were included, which was justified by the accuracy and symmetry of the applied wire erosion process to manufacture the monolithic mechanism.

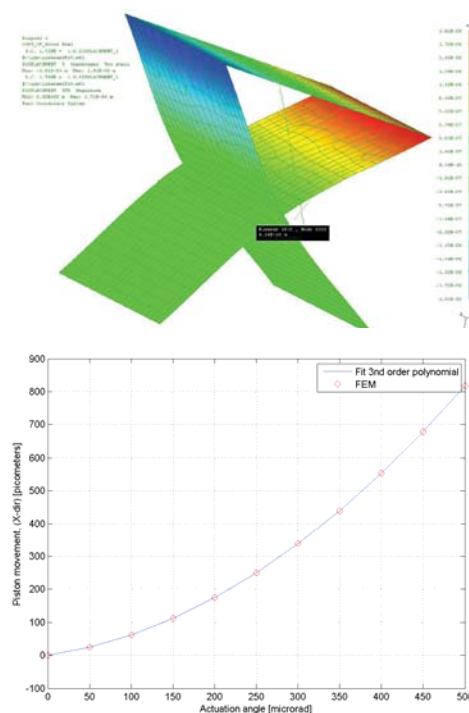


Figure 3: Top: Meshed FEM model of the Haberland hinge, actuated to an extreme angle. Outcome of the FEM analysis is the longitudinal and lateral jitter of the axis of rotation. Production tolerances of  $\pm 10 \mu m$  are taken into account. Bottom: The piston movement of the axis of rotation under different actuation angles. By taking the derivative of the fitted polynomial, the piston sensitivity can be determined for different angles.

A finite-element model analysis (FEM) of the Haberland hinge was used to predict the longitudinal jitter, caused by the coupling between angular jitter and piston sensitivity.

Production tolerances of  $\pm 10 \mu\text{m}$  were included, which was justified by the accuracy and symmetry of the applied wire erosion process to manufacture the monolithical mechanism.

#### F. Electrical design

For the actuation, two piezo stacks (PPA20M) of Cedrat Technologies are used. For the stroke of  $20 \mu\text{m}$ , and with the limitations on magnetic materials, a piezo stack is the most appropriate actuator. The stacks are driven with a high voltage piezo amplifier (Cedrat Technologies LA75B), which produces voltages between  $-20$  and  $+150 \text{ V}$ .

Because of piezo hysteresis and discharge behaviour, a closed loop system is required to meet the requirement for angular jitter in the entire range. The controller acting between the sensor and piezo actuator can have a low bandwidth, because only disturbances within the LISA measurement band width have to be suppressed.

The sensor consists of an active target capacitive sensor system, which measures the displacement of the far end of the mirror (see

Figure 4). The tilting of the mirror is less than  $0.5 \text{ mrad}$ , which has only a small influence on the capacitive sensor signal. A one-time calibration ensures that the sensor signal is representative of the mirror angle with high enough accuracy. The active target system is preferred over a passive target system for the following reason: in a passive target system, the cable capacitance is in parallel to the capacitance to be measured, and is typically a few orders higher. This makes it very sensitive to low frequency environmental changes which dramatically influence the cable capacitance. In an active target system, the target is connected to a virtual ground, which draws the current from the cable capacitance. This way, the system will be much less sensitive to environmental changes.

The capacitive probe is a standard Lion Precision probe, whereas the active target consists of an isolating BK7 plate, coated with a layer of gold. The active target, located on the moving part, is connected to the sensor cable by two thin copper wires, which add negligible parasitic stiffness to the Haberland Hinge. The capacitance-to-digital converter (CDC) electronics were chosen to be a custom electronics board, especially for extreme requirements on low frequency noise.

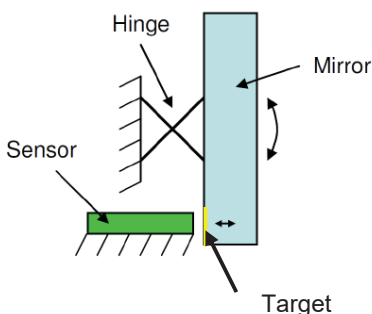


Figure 4: Schematic illustration of the active target capacitive sensor. The sensor measures the displacement of the tip of the mirror. The tilting of the mirror is taken into account by one-time calibration.

Typically, capacitive sensor electronics introduce  $1/f$  type noise in the amplification, but the charge-integration configuration and precision electrical components chosen for the CDC board reduced this effect maximally.

#### G. Sensor noise testing

Due to the closed loop operation of the PAAM and the low frequency performance requirements, the most critical noise source in the loop is the capacitive sensor. To test the performance of the CDC board in combination with the active target capacitance, a test set-up was designed to measure the noise. A stable reference capacitance was placed in a temperature ( $\pm 1 \text{ K}$ ) and humidity controlled environment, while the CDC board was kept in a normal laboratory environment.

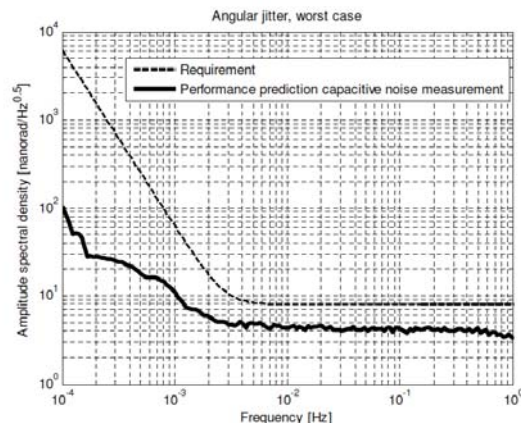


Figure 5: Performance prediction of the angular jitter, based on capacitive noise measurements under controlled environmental conditions. A dynamical model of the PAAM and the controller is included. The predicted performance is below specification.

The resulting contribution of the electrical noise to the angular jitter in terms of amplitude spectral density is shown in Figure 5, calculated from the measurement using a simple model of the plant and a controller with a bandwidth of approximately  $10 \text{ Hz}$ . In worst case, the capacitive sensor noise is low enough to achieve the required performance. Especially the low magnitude of  $1/f$  type noise is a remarkable performance achievement for a displacement sensor. Noise measurements of other electrical components in the control loop resulted in noise levels that were much lower than the capacitive sensor noise within the band width of interest. It is therefore justified to consider the noise level of the capacitive sensor as a total performance prediction.

#### H. Environmental testing

The specification for the launch loads is  $25 \text{ g RMS}$ . This random vibration load is applied to the Elegant Bread Board realization of the PAAM. The spectrum containing  $25 \text{ g RMS}$  was notched because of a lower Q-factor of the mechanism. In three translational degrees of freedom, an effective spectrum of approximately  $20 \text{ g RMS}$  was applied by a shaker. The

response, measured with tri-axial accelerometers, showed no significant shift of resonance frequencies. After testing, visual inspection of the mechanism showed no degradation.

### I. Performance testing

The performance of the Elegant Bread Board realization of the PAAM was measured with the help of the Albert Einstein Institute in Hannover, because of their experience with measuring picometer stabilities and the availability of an existing measurement facility<sup>2</sup>. For details on the Performance measurement setup see [2].

#### 1) Test description

Two of the critical requirements of the PAAM need to be verified by tests: the OPD and the angular jitter. Both are measured at three different static angles within the range of the mechanism. The LISA measurement band width determines the length of each performance measurement: the lowest frequency to be measured is 0.03 mHz. With several repetitions of this period to obtain a proper spectral estimate, the measurement time per angle is approximately 48 hours.

To measure the OPD, the PAAM has to be aligned accurately in the resonance cavity. To achieve this, a modulation sine wave is used as a set point on the mechanism, which will follow this signal by rotation of the mirror. Through the amplitude of the sine wave, the misalignment of the axis of rotation with respect to the incoming beam can be estimated.

To measure the angular jitter, the PAAM is deliberately placed at an alignment offset. A modulation sine wave is used as a set point for the PAAM. Through the amplitude of the sine wave, the coupling of angular jitter to OPD can be estimated. A long measurement of OPD will then provide an indirect measurement of the angular jitter of the PAAM.

#### 2) Test performance results

The results of the performance measurements of OPD and angular jitter are shown in Figure 6. For all angles, the performance of the mechanism is exactly according to the requirements. The peak visible at 50 mHz is the modulation sine wave which is used for alignment in the OPD measurements, and coupling estimation in the angular jitter measurements.

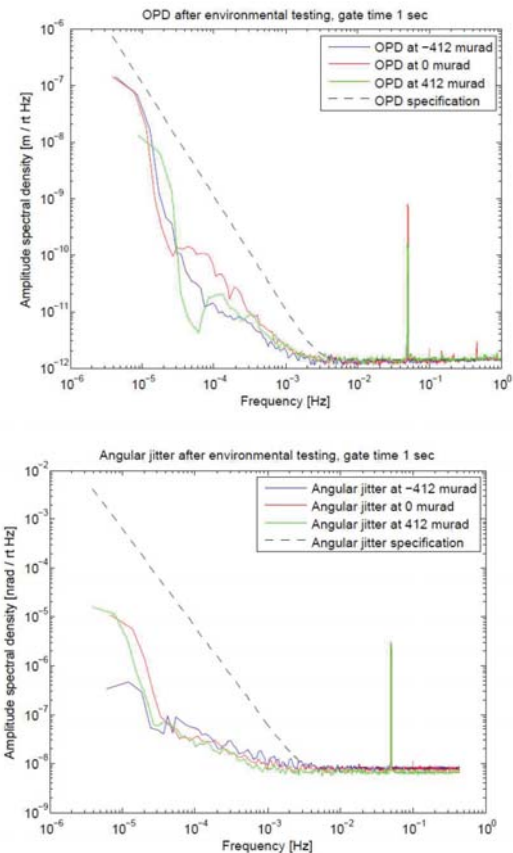


Figure 6: Top: Amplitude Spectral Density of the OPD measurements on the PAAM. For all angles, the result meets the requirements. The peak at 50 mHz is introduced for alignment in the cavity. Bottom: Amplitude Spectral Density of the angular jitter measurements on the PAAM. The PAAM is deliberately placed at an alignment offset, to make the angular jitter dominant in the OPD measurement. For all angles, the result meets the requirements. The peak at 50 mHz is introduced to estimate the coupling of angular jitter to OPD.

### J. Conclusion

With the design, realization and testing of the PAAM, TNO Optomechanics has demonstrated that a scanning mechanism with picometer stability and under extreme environmental conditions is achievable. Performance test measurements have shown that it is compliant with the challenging requirements for optical path delay and angular jitter.

The analysis, as well as the measurement results, shows that application of a Haberland hinge in a monolithic structure enables rotation with negligible parasitical motion in terms of OPD. The thermal design of the structure showed to be sufficient to guarantee the thermal stability.

The angular jitter measurements have shown that an active target capacitive sensor system meets the extreme requirements on low frequency noise.

The Elegant Bread Board of the PAAM, as used in the performance testing, will be included in a bread board model of the LISA Optical Bench in the near future.

III. FIBER SWITCHING UNIT ACTUATOR

A. Introduction

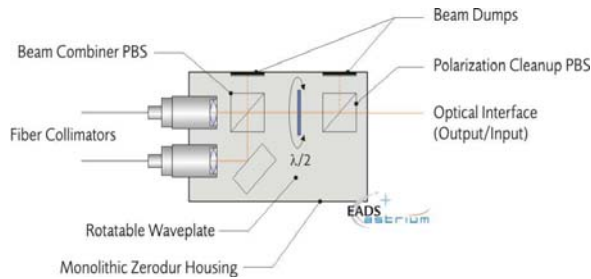


Figure 7: The chosen Fiber Switching Unit Concept.

The Fiber Switching Unit Actuator is part of the Fiber Switching Unit as shown in the figure below. The aim of the FSU is to allow the optical bench to switch between two separate laser sources, one a redundant backup for the other. The lasers, and fiber feeds to the optical bench should be separate to give the maximum possible levels of failure robustness.

The aim of the Fiber Switching Unit Actuator is to hold and rotate the half wave plate of the FSU.

B. FSUA requirements

To switch between two separate laser sources a rotation of 45 degrees of a half wave plate is mandatory. The main functionalities of the FSUA are:

- To hold the half wave plate with a sufficient stability.
- To actuate the half wave plate over 45 degrees around the optical axis in order to switch from primary to the redundant laser source with sufficient accurate repeatability of the FSU outgoing beams.

The following requirements were considered to be design driving:

- For the outgoing beams to be collinear better than 1 micrometer the tip tilt of the wave plate has to be better than 0.5 millirad over the full stroke. 0.25 millirad is used for the alignment of the wave plate with respect to the rotation axis of the actuator and 0.25 millirad is used for the wobble of the actuator itself.
- The angular jitter of the FSU output beam shall not exceed  $4 \mu\text{rad}/\sqrt{\text{Hz}}$  within the LISA MBW.
- The dimensions of FSUA shall be 42 x 60 x 27 mm<sup>3</sup> maximum. The output face shall be on the short side.
- The FSUA storage and transportation temperature range shall be 0°C to +50° C.
- A sub system on the OB should survive acceleration loads of 75g Quasi static.

- Survive the launch conditions as specified below without degradation of performance or alignment stability.

Equipment axis	Frequency [Hz]	
All axes	20-100	+ 3dB/oct
	100-300	PSD(M) = 0.05 × (M+20 kg)/(M+1 kg) g <sup>2</sup> /Hz
	300-2000	- 5dB/oct
	Duration	2.5 min/axis

Figure 8: The random vibration levels according to the ECSS

- Survive a shock load as specified below without degradation of performance or alignment stability (Q=10).

Frequency [Hz]	SRS value in [g]
100	20
1500	1000
10000	1000

Figure 9: The shock levels

C. FSUA design

1) Working principle of Piezo inertia actuator.

The FSUA is developed in a close cooperation with Attocube AG and based on the piezo sliding concept. THE FSUA is powered using slip-stick motion. See figure below for schematic sketches of a translational version of a piezo inertia actuator.

The basic principle of rotation stages based on slip-stick inertial motion is the controllable use of the inertia of a sliding rotator. In the FSUA, the sliding block slips along a rotational guide to which it is otherwise clamped (sticking) in frictional engagement. To obtain a net step, the guiding rod is first accelerated very rapidly over a short period of time (typically microseconds) so that the inertia of the sliding block overcomes the friction. This way, the sliding rotator disengages from the accelerated rod and remains nearly non-displaced. Subsequently the guiding rod moves back to its initial position slowly enough so that the sliding rotator this time sticks to it and thus makes a net step. Periodic repetition of this sequence leads to a step-by-step motion of the sliding rotator in one direction. A piezo electric ceramics pushes or pulls the rotational guiding and the exact sequence in the slip and stick motion is controlled by an appropriate voltage signal.

2) Implementation of piezo inertia principle in the FSUA

Two redundant pairs of 2 piezo stacks are connected to rotational elastic guiding, see figures below for details. On this elastic guiding a rotating inertia is preloaded and guided by sliding rotational contact. On this rotating inertia a half wave plate is mounted iso-statically. When 2 of the 4 piezos are actuated, relative fast, the elastic rotational guiding will rotate. Due to combination of the high inertia, fast rotation and relative low friction force between elastic guiding and rotating

inertia slip will occur between the elastic guiding and the rotating inertia. This fast movement in one direction is followed by a slow movement in the opposite direction.

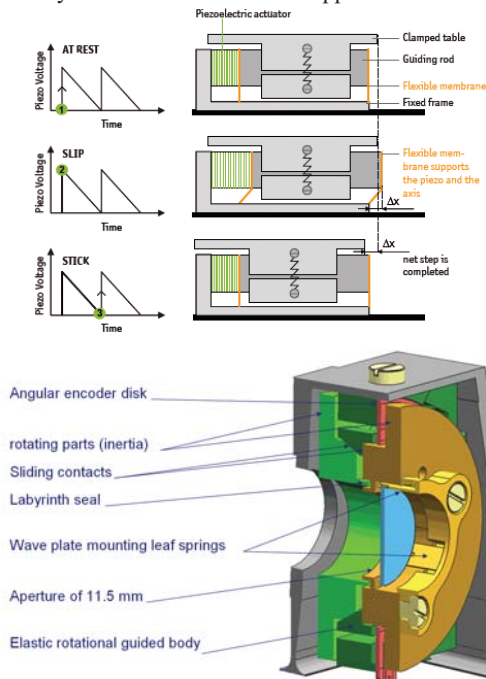


Figure 10. Top. Schematic sketches of the working principle of a linear piezo inertia actuator. (Picture courtesy of Attocube) Bottom: A cross section of the piezo inertia actuator in its housing. The labyrinth seal together with the potentiometer are implemented in the FSUA. The aim of the labyrinth seal is to keep possible debris generated in the actuator contact or potentiometer away from the optics. The aim of the potentiometer is to detect the wave plate orientation. The two rotating parts are preloaded on the drak green rotation stage with limited stroke with a defined preload.

During this slow movement no slip occurs and thereby a step between the elastic guiding and rotating inertia is made. By repeating the fast movement in one direction followed by a slow movement in the opposite direction large rotation angles of the wave plate can be made. To measure the position of the wave plate a potentiometer is integrated in the actuator. To further minimize the risk of contamination of the optics a labyrinth seal is places in between the sliding contact and the wave plate. A life test and an inspection after this test have been performed on the FSUA. The piezo inertia actuator is mounted to the housing; this housing is mounted iso-statically to the Zerodur Optical Bench.

Some properties of the FSUA:

- Envelope is h=41mm x w=41mm x l=26mm.
- The mass is approximately 100 grams.
- The design doesn't require a launch lock, rotation of the wave plate due to vibration loads do occur.
- No permanent magnets nor ferromagnetic materials are used.

- In the sliding contact a MoS2 coating is used. Life testing is performed;
- The actuator is redundant; 2 pairs of 2 piezo actuators.
- External alignment tools are used to alignment of the wave plate with respect to the rotation axis of the actuator;
- The wave plate is mounted iso-statically to survive thermal environment and to reduce disturbance of the optical surface due to thermal or other effects.

#### D. FSUA performance and environmental verification

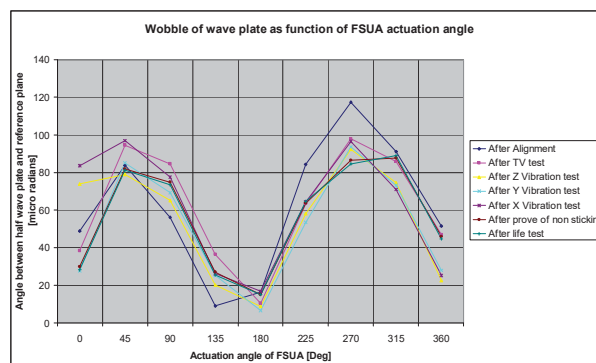


Figure 11: Wobble measurement of the first model of the FSUA after the life test. Wobble is still well within specified +/- 500 micro radians over 45 degrees of actuation.

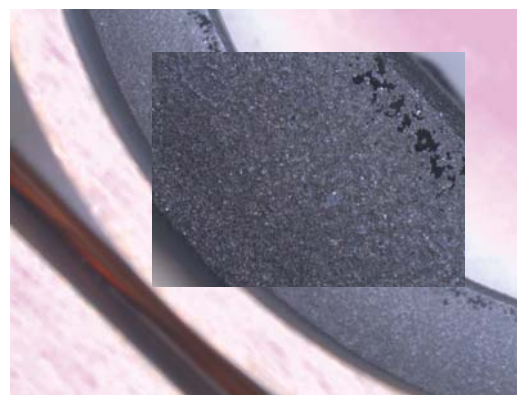
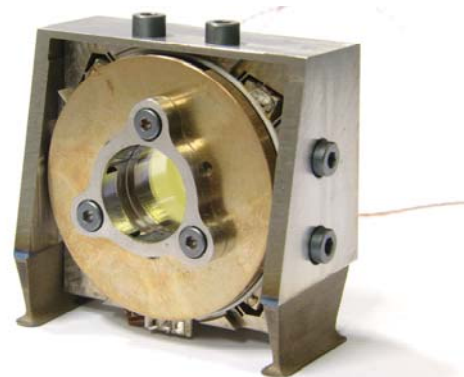


Figure 12: Top: The FSUA with integrated angular measurement system. Bottom: a photo of one of the sliding contact surfaces after the life test no signification degradation of the surface.

On the first model of the FSUA Vibration tests, Thermal cycling tests and a life test is performed, in between all tests steps the wobble performance of the mechanism is determined, see figure above for the results.

#### E. Conclusion

With the design, realization and testing of the FSUA, TNO Optomechatronics in cooperation with Attocube AG has demonstrated that in very limited available space it is possible to actuated a wave plate with a wobble less than  $\pm 75$  micro radians, leading to a beam jitter of less ten  $\pm 75$  nm. It is also shown that the mechanism will survive the launch and thermal vacuum loads. The life test performed inside and outside vacuum shows no measurable degradation in performance of the FSUA.

Two mechanisms have been build and tested, ready to soon be integrated on the LISA/NGO optical bench EBB [3,4]

### IV. IN FIELD POINTING MECHANISM

#### A. Introduction

Due to seasonal orbit evolution effects on the relative positions of the three spacecraft, the outgoing laser beam angles have to be corrected with a stroke of  $\pm 2.5^\circ$ . Critically important are the contribution to the optical path length, which has to be lower than  $3 \text{ pm} / \sqrt{\text{Hz}}$ , and the angular jitter, which has to be lower than  $1 \text{ nrad} / \sqrt{\text{Hz}}$ , both while the IFPM is scanning with a low constant velocity. Another driving requirement is the redundancy.

#### B. Actuator performance testing

As with the PAAM, the mechanical concept is based on a mirror bonded to a monolithic structure, which allows rotation of the mirror by two elastic Haberland hinges. The axis of rotation is located in the plane of the mirror, thereby minimizing the coupling between angular jitter and optical path length.

As electromagnetic actuation is not allowed on the optical bench, the number of actuation options is reduced strongly. Electrostatic actuation is ruled out because of the holding and actuation force requirements. Piezo-stacks are ruled out because of the large stroke requirement. Other concepts, such as thermal or hydraulic actuation, are ruled out because of stability, heritage and resolution problems.

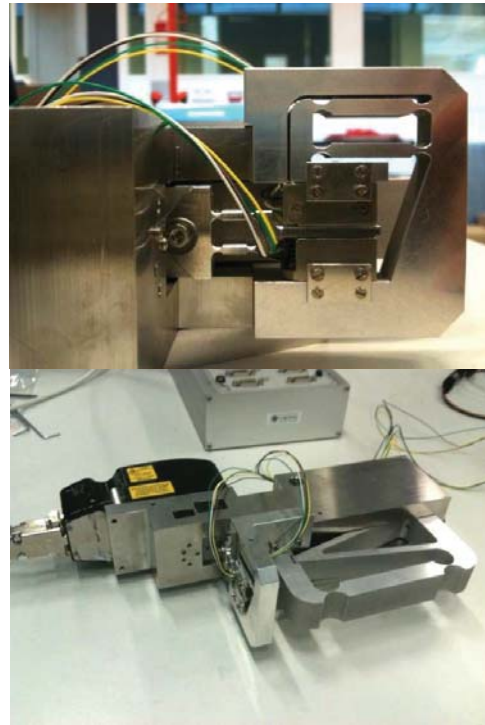


Figure 13: Picture of the piezo-stepper test set-up, to measure the errors during constant velocity motion, introduced by stepping.

The most suitable actuator principle is a piezo-stepper, which has an unlimited stroke, but also a very fine resolution because of the analog mode option. This actuator is tested in a dedicated test set-up, in which the jitter during stepping is optimized and measured. The test set-up design, as shown in the figure above, features two opposing steppers with each 4 legs, pressed together by an elastic pre-stress configuration. Between the legs of the two steppers, a walking rod is pushed forward. The rod is attached to a large stroke elastic linear guidance, of which the displacement can be measured by a differential interferometer (Renishaw DI).

Four high voltage amplifiers, one for each stepping phase, are controlled by a dSpace system that uses feedback from the interferometer. The shape of the voltage signals determining the stepping phases, is optimized to enable constant velocity motion with very low disturbances. The optimized voltage shapes are based on [7]. By using an asymmetric waveform, in which the contact part of the stepping motion is significantly longer than the non-contact part, the contact parts of each leg tip overlaps, and the velocity does not drop to zero anymore. This way, a more continuous velocity can be achieved.

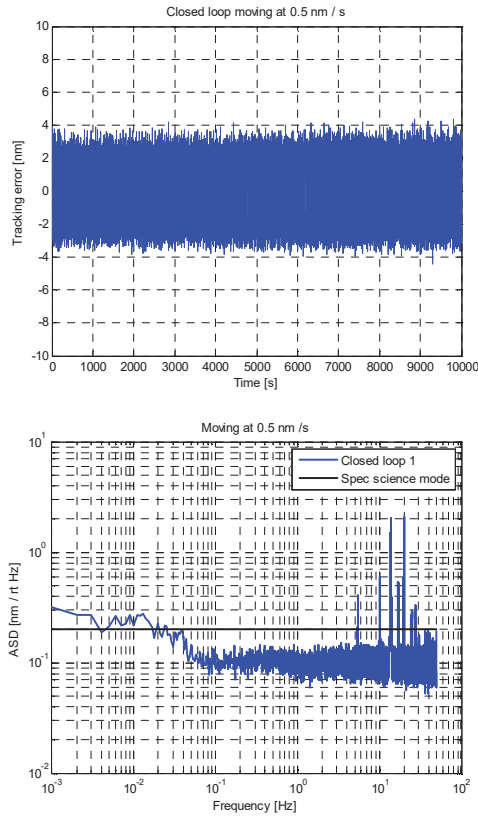


Figure 14: Top: Time domain result of the tracking error of the piezostepper set-up during 10000 seconds of 0.5 nm/s motion. Bottom: Amplitude spectral density of the tracking error of the piezostepper set-up, during 10000 seconds of 0.5 nm/s motion.

Measurements of the angular jitter during 0.5 nm/s (science mode) and 20 μm/s (beam acquisition mode) motion are performed. To make sure steps are performed during the measurement, a measurement time of 10000 seconds is used.

Figure 14 Top shows the tracking error of the piezo-stepper set-up in the time domain, while Figure 14 Bottom shows the spectrum, as compared to the requirement.

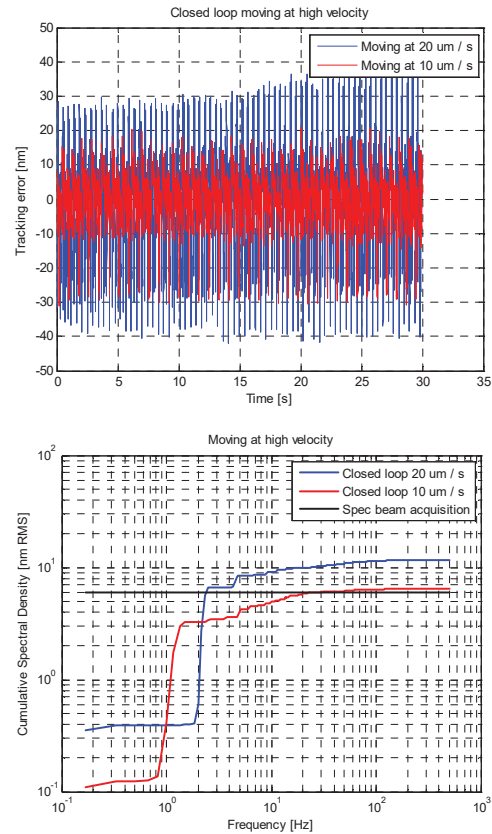


Figure 15: Top: Time domain result of the tracking error of the piezostepper set-up during 30 seconds of 10 and 20 μm/s motion. Bottom: Cumulative Spectral Density of the tracking error of the piezostepper set-up during 30 seconds of 10 and 20 μm/s motion.

The peak to peak tracking error is within ±5 nm. In the frequency domain, the low frequency noise is above the specification for angular jitter in science mode (corrected for the rotation arm). Above 5 Hz, there are some sharp peaks above the specification for angular jitter in science mode.

The tracking error during beam acquisition mode is also measured. Figure 15 Top shows the tracking error during 10 and 20 μm/s motion. The peak to peak error is approximately ±40 nm. Figure 15 Bottom shows the integration of the amplitude spectral density, showing the rms of the tracking error in beam acquisition mode. Below 500 Hz, the total contribution to the error is out of spec, but below 10 Hz the angular jitter is within 6 nm RMS.

As can be concluded from the test results, not all performance requirements are achieved. However, the performance is very close to the requirement, and with small adjustments to the design of the actuator configuration, we believe the angular jitter requirements can be fulfilled.

### C. IFPM design

With the knowledge from the piezostepper set-up, and additional requirements on the launch loads and redundancy, the piezostepper is integrated in the IFPM steering mirror concept. A CAD picture of the design is shown in Figure 16.

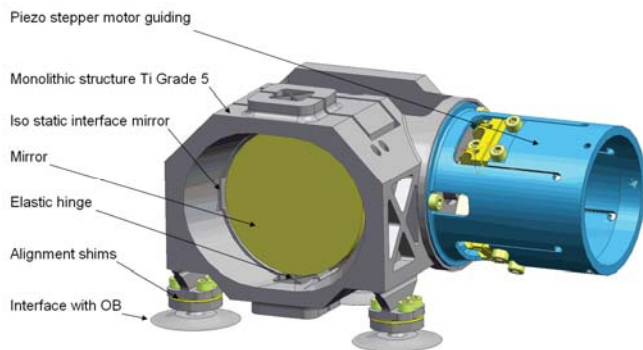


Figure 16: CAD picture of the IFPM beam steering mirror design, including redundant piezo steppers.

Some properties of the mechanism:

- The mirror guiding is provided by a haberland hinge, simple and stable, also used in the PAAM.
- Actuation is done by a TNO build piezomotor. Standard components are used as active elements.
- The preloading and precision guiding is done by 3 leafsprings. Function of pre loading and guiding are combined to minimize complexity and the number of components.
- Motor is semi iso-statical mounted on the mechanism and can be removed.
- The piezo stepper walks over a triangular ceramic bar which is connected to the rotating
- 2 optical encoders of MicroE will measure the angle of the mirror.

### V. CONCLUSIONS

The actuator measurements and mirror surface measurements [9] in combination with the experience from the PAAM mechanisms and the performed analyses give us sufficient confidence to start built and test the IFP Mechanism.

Currently the IFPM parts are being manufactured, TNO expects to deliver the mechanism to Astrium EADS Friedrichshafen before the end of the year to start the performance measurements [10] the beginning of 2013.

### VI. ACKNOWLEDGMENTS

TNO likes to thank ESA and NSO for their funding for the development of the PAAM, FSUA and IFPM. We also like to

thank Albert Einstein Institute, University of Glasgow, University of Delft and Attocube AG. Special thanks goes to Astrium EADS Friedrichshafen.

### VII. REFERENCES

- [1] Danzmann, K., "LISA Mission Overview", *Advances in Space Research* Vol. 25, Issue 6, 2000, 1129 – 1136
- [2] Troebs, M., "Laser development and stabilization for the spaceborne interferometric gravitational wave detector LISA", PhD Dissertation, 2005.
- [3] d'Arcio, L., e.a., "An Elegant Breadboard of the Optical Bench for LISA/NGO" *LISA Symposium 2012*, Paris.
- [4] Trobs, Michael; et al; Testing the LISA Optical Bench, *LISA Symposium Paris 2012*
- [5] Pijnenburg, J., Rijnveld, N., Sheard, B., "Picometer stable scan mechanism for gravitational wave detection in space: LISA PAAM" *38th COSPAR Scientific Assembly*, volume 38, pages 3758--+, 2010.
- [6] Pijnenburg, J., Voert, te M., e.a., "Ultra stable iso-static bonded optical mount design for harsh environments", *Proc. SPIE 8450* (2012).
- [7] Merry, R., e.a., "Using a Walking Piezo Actuator to Drive and Control a High-Precision Stage", *IEEE/ASME Transactions on mechatronics*, Vol. 14, No. 1, February 2009
- [8] D. Weise, P. Marenaci, P. Weimer, M. Berger, H. R. Schulte, P. Gath, and U. Johann. Opto-mechanical architecture of the LISA instrument. *ICSO Conference Proceedings*, 2008.
- [9] Harald Kögel, Martin Gohlke, Joep Pijnenburg, Thilo Schuldt, Ulrich Johann, Claus Braxmaier and Dennis Weise "Interferometric Surface Characterisation with Sub-Nanometer Reproducibility for Enabling a Correction of Pathlength Errors Resulting from Mirror Surface Topography". *ICSO Conference Proceedings*, 2012.
- [10] T. Schuldt, M. Gohlke, D. Weise, U. Johann, A. Peters, C. Braxmaier: "Picometer and nanoradian optical heterodyne interferometry for translation and tilt metrology of the LISA gravitational reference sensor" *Class. Quantum Grav.* 26 085008 (2009)
- [11] Weise, D., e.a., "An Elegant Breadboard of the Optical Bench for LISA/NGO", *ICSO 2012 Conference Proceedings*.  
Typically, capacitive sensor electronics introduce 1/f type noise in the amplification, but the charge-integration configuration and precision electrical components chosen for the CDC board reduced this effect maximally.